14.1 ON THE ROLE OF DESCENDING RAIN CURTAINS IN TORNADOGENESIS

Amanda K. Kis#, Jerry M. Straka* and Katharine M. Kanak
University of Oklahoma, Norman, Oklahoma
#Storm Prediction Center, Norman, Oklahoma

1. INTRODUCTION

Knowledge of the environmental conditions that promote mid-level mesocyclogenesis is insufficient for predicting tornadogenesis. High accuracy of forecasts of environments favorable for supercell formation, but a nearly 75-percent failure rate of tornado warnings based on the presence of a mid-level mesocyclone (Trapp et al. 2005) reflect this dichotomy.

In this study the role of descending rain curtains in producing strong rotation at the ground and tornadogenesis is investigated and is an extension of some of the axisymmetric work of Davies-Jones (2008; herein DJ08). The work herein differs from DJ08 in that it is in three dimensions.

In section 2, several theories of tornadogenesis are summarized for comparison. In section 3, the three-dimensional numerical model set-up and initial conditions used to simulate mature supercell are described. Whilst most tornado simulations in the literature are axisymmetric, the addition of a third-dimension in idealized simulations (e.g.,Walko 1993; and Lewellen and Lewellen 2002.) allow asymmetries to develop and evolve. First a control run is described for a given amount of rain based on that proposed by DJ08. Then experiments are discussed that have both the amount of precipitation in the rain curtains vary and the geometry of the rain curtains vary from the control run. The latter of these are an effort to simulate supercells in which the so-called "clear slot" associated with the rear flank downdraft initially does not wrap completely around the region of the incipient tornado. The experiments and their resulting successes or failures in producing tornadogenesis are evaluated in section 4, and conclusions are highlighted in section 5.

2. BACKGROUND

Given the presence of a mid-level mesocyclone, one hypothesis for tornadogenesis is the dynamic pipe effect (DPE) (Leslie 1971; Trapp and Davies-Jones 1997) in which it is assumed that tornadoes are downward-building extensions of the mid-level mesocyclone characteristic of parent supercells. Morton (1966) argued that a vortex aloft in cyclostrophic balance, in which vertical motions are permitted, but radial motions are inhibited by the cyclostrophic balance, draws air inward at the lower end of the vortex "like a pipe". Subsequently, cyclostrophic balance is established at the lower end of the vortex in a progressive manner in which the radial inflow occurs at lower and lower levels. The DPE is possible in the presence of sufficient ambient vertical vorticity on the mesocyclone scale that can be concentrated into a tornado by radial convergence (Smith and Leslie 1979).

Doppler radar observations of "descending" and "nondescending" tornado vortex signatures (TVS) suggest that only half of tornadoes form possibly by the DPE (Trapp et al. 1999). The other half is associated with tornadogenesis independent of the mid-level mesocyclone (Trapp and Davies-Jones 1997). The tornadoes that might form by the DPE are characterized by descending TVSs, and those that form otherwise are characterized by nondescending TVSs. Nondescending TVSs occur when ambient vertical vorticity is insufficient for the DPE, but vertical vorticity is maximized near the surface by perhaps horizontal shear (Trapp and Davies-Jones 1997).

Davies-Jones (1982a,b) hypothesized that a downdraft is necessary to produce and concentrate positive vertical vorticity next to the surface when pre-existing vertically oriented rotation is absent. Besides tilting horizontal vorticity into the vertical, subsidence in the downdraft transports air with high vertical vorticity to the surface. Subsequent studies (e.g. Walko 1993) also have shown that a downdraft is necessary in some cases for tornadogenesis.

Other studies began to examine the role of baroclinic vorticity generated solenoidally along rain-cooled outflow (e.g., Rotunno and Klemp 1983; Klemp and Rotunno 1985). Davies-Jones and Brooks (1993) hypothesized that streamwise horizontal baroclinic vorticity was generated near the surface along rain-cooled outflow from the RFD. This vorticity is reoriented vertically by baroclinity in the downdraft outflow and is ingested by the updraft, and amplified by stretching into a tornado at the ground.

Interestingly a surface baroclinic zone was not detected on the forward flank near several significant tornadoes using fine scale surface observations (Markowski et al. 2002; Shabbott and Markowski 2006). Additionally, Markowski et al. (2003) demonstrated numerically that strong surface baroclinicity along rain-cooled air is not necessary for tornadogenesis. Tornado intensity increases as the buoyancy of downdraft parcels increases. Buoyancy is maximized with relatively low LCLs (i.e. relatively high boundary layer relative humidity) and a moderate amount of precipitation. As static stability increases, vertical motion is inhibited.

Observational and numerical studies highlight the connection of the rear flank downdraft (RFD) to tornadogenesis (for a review, see Markowski 2002). Descending precipitation within the RFD is of additional importance to tornadogenesis. The hook echo signature often derives its existence from descending precipitation in the RFD (Markowski

Corresponding author address: Jerry M. Straka,
Univ. of Oklahoma, School of Meteorology,
Norman, OK 73072; e-mail: jstraka@ou.edu

2002), and is in many instances a precursor to tornadogenesis (Rasmussen et al. 2004). Going back in history, it is noted that Fujita (1975) observed descending precipitation from the RFD "streaking" into the tornadic region of the 1974 Xenia, Ohio storm (Fig. 1), and as a result he formed the following hypothesis.

Fujita (1975) described a process by which the RFD and descending precipitation promote tornadogenesis. First, subsiding air in the downdraft is re-circulated into the developing tornado, producing strong convergence on the backside of the developing tornado. Then, precipitation descends through the RFD and transports angular momentum downward. Air and precipitation enters and is "recycled" into the developing tornado cyclone circulation, increasing the tangential acceleration. These steps became known as Fujita's Recycling Hypothesis. Subsequent studies (e.g. Markowski et al. 2002) use the term "recycling" to describe air parcels ascending a few kilometers from the storm, entering a downdraft that transports them to the surface, and re-entering the updraft through the (developing) tornado.

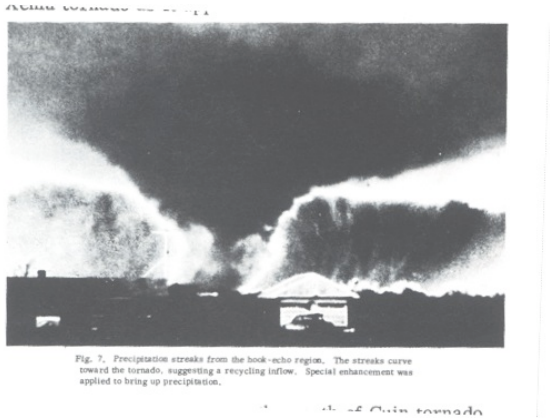

Fig. 7. Precipitation streaks from the hook-echo region. The streaks curve toward the tornado, suggesting a recycling inflow. Special enhancement was applied to bring up precipitation.

Fig. 1: Precipitation streaks from the hook echo region. The streaks curve toward the tornado, suggesting a recycling inflow. Special enhancement was applied to bring up precipitation. (From Fujita 1975).

With these findings, attention more recently has returned to the role of barotropic vorticity in tornadogenesis. Markowski et al. (2003) and DJ08 demonstrated a purely barotropic mechanism of tornadogenesis in axisymmetric models, in which a descending rain curtain instigates tornadogenesis. Rain diverges from the updraft apex in DJ08, descends from the top of the storm along the updraft-downdraft interface in an annular, precipitation-driven downdraft. Markowski started his rainy downdraft a couple of km up from the ground and away from the updraft. In both cases these descending rain curtains dragged air with high angular momentum to the surface. This increased tangential acceleration and created positive vertical vorticity next to the surface near the center of the updraft. Then, upward recycling of high angular momentum air by the low-level updraft amplified the vertical vorticity through stretching and eventually resulted in tornadogenesis. These steps essentially describe Fujita's Recycling Hypothesis, and are pictured in Fig. 2.

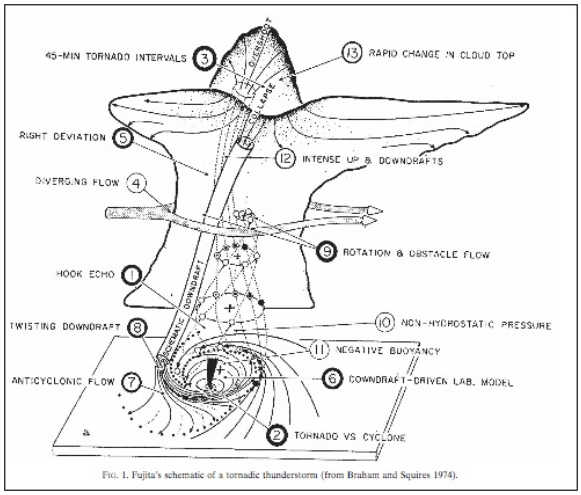

Fig. 2: Fujita's schematic of a tornadic thunderstorm (From Braham and Squires 1974).

DJ08's and Markowski et al.'s (2003) models both emphasized the importance of descending precipitation to tornadogenesis. In these simulations the formation of features observed in tornado producing parent supercells—including the tornado cyclone and collapse of the updraft top—lend credibility to these results. Lewellen & Lewellen (2007) suggest that descending precipitation in the hook echo might passively produce a tornado by blocking low-level inflow and instigating dynamic corner flow collapse as an explanation for the results of these simulations in real tornadogenesis.

3. METHODOLOGY

3.1 Numerical model description

Straka's Atmospheric Model (SAM) is a three-dimensional, fully compressible, non-hydrostatic model. For this study, SAM is employed with the incompressible Navier-Stokes equations. A quadratic conserving, second-order centered-in-space "box" finite difference scheme is used for scalars and velocities. A centered-in-time Leapfrog finite difference scheme is used for temporal integration. A sixth-order numerical filter and divergent damping are also applied. The model is run using MPI on a massively parallel architecture.

3.2 Experimental Design

3.2.1. Domain Parameters

The non-rotating domain is 20 km x 20 km x 12.2 km, with both horizontal and vertical grid spacing of 100 m. As in DJ08, this domain is sufficiently large to

model both the parent supercell and tornado. The lateral boundaries are open as in Klemp and Wilhelmson (1978) but with no intrinsic gravity wave velocity for outflow (dry adiabatic sounding). Lewellen and Lewellen (2007) note that an open domain may be dangerous if the simulated storm becomes so strong as to force unknown feedbacks outside the domain. However, since the downdraft is entirely within the domain, inflow does not enter through the lateral boundaries. The upper boundary is closed and rigid. The lower boundary is impermeable, free-slip, and rigid. As in DJ08, Fick's first law is invoked for diffusion and is used for the sub-grid turbulence closure scheme, with a mixing coefficient of K = 100 m^2 s^{-1}. A comparison of these values with those of DJ08's simulation is summarized in Table 1.

	Δx (m)	Δz (m)	L_z (km)	$L_x = L_y$ (km)	K_m (m^2 s^{-1})
SAM	100	100	12.2	20	100
DJ08	42	42	12	16.9	204

Table 1: Domain parameters in SAM as compared with DJ08.

3.2.2. Initial Condition

The thermodynamic base state profile is dry neutral, with θ_0 = 300 K. Density is held constant at 1 g kg^{-1} throughout the domain. With these conditions, no baroclinic vorticity can be produced.

The initial flow is Beltrami, and approximates a steady, mature supercell with cyclonically rotating updraft (with rotation maximized at mid-levels) surrounded by an anticyclonically rotating downdraft. The equations governing the initial Beltrami flow are detailed in Section III of DJ08, cast here in Cartesian coordinates and with the decay term neglected. The velocity fields are prescribed according to the following equations:

$$u_o = -(\mu / k) W_o J_1(k\sqrt{x^2 + y^2}) \cos(\mu z) \quad (1)$$

$$v_o = (\lambda / k) W_o J_1(k\sqrt{x^2 + y^2}) \sin(\mu z) \quad (2)$$

$$w_o = W_o J_o(k\sqrt{x^2 + y^2}) \sin(\mu z) \quad (3)$$

where W_0 is the initial maximum upward velocity. The value of W_0 also serves as the thermodynamic speed limit (Fiedler and Rotunno 1986). These equations describe a helical flow, where u, v, and w are the three-dimensional wind components, x, y, and z are the three Cartesian directions, λ is the constant rate at which the wind veers with height, μ is π/L_z, k = $(\lambda^2 - \mu^2)^{(1/2)}$, J_0 is the Bessel function of zero order (six terms retained), and J_1 is the Bessel function of first-order (six terms retained).

Initial amplitudes of u_0, v_0, w_0, perturbation vertical vorticity (ζ'_0), and perturbation pressure (p'_0) are specified in Table 2, and compared to those of DJ08. DJ08 truncated the equations at the first zero of the Bessel function. This study, however, retains the full equations to the limits of the domain. This prevents unrealistic interactions of the vortex with the boundaries. The resulting initial flow is pictured in Fig. 3. This initial flow is slightly off-center, which results in slight storm tilt with height as the simulations progress.

	Max{u_0}	Min{u_0}	Max{v_0}	Min{v_0}
CR	22.8	-22.8	22.8	-22.8
DJ08		-22.9	22.9	
	Max{w_0}	Min{w_0}	Max{ζ'_0}	Min{ζ'_0}
CR	34.0	-13.7	1.78×10^{-2}	-7.2×10^{-3}
DJ08	34.0	-13.7	1.80×10^{-2}	-7.2×10^{-3}

Table 2: Comparison of initial Beltrami amplitudes between our control run and DJ08's simulation. Values for DJ08 are taken from Table 1 of DJ08. Note that DJ08 does not list values of Max{u_0} and Min{v_0}.Units of u_0, v_0, and w_0 are m s^{-1}. Units of ζ'_0 are s^{-1}. Units of θ_0 are K.

As there is no body force / latent heat release, and no continuous updraft is defined (as in Lewellen et al. 1997) only tornadogenesis is simulated. Upon tornadogenesis, the downward directed pressure gradient force drives a downdraft down the center of the axial updraft, and results in the dissipation of the tornado owing to the lack of a continuously forced updraft. Thus, as in DJ08, tornado maintenance and decay are not simulated.

Hydrometeors are characterized by liquid water only (i.e. they are characterized by a fall speed and drag only). Drops are assumed to be large (a few mm in diameter) and fall quickly (about 8.5 m s^{-1}) so that evaporation is minimal and can be assumed to be negligible. Hydrometeors are released at the first time-step and thereafter. The rain mixing ratio, q, is specified as circular disc atop the cyclonic circulation. It is maximized, with a value of q_{max}. It then varies outward as:

$$q(x, y, z_{top}, t) = q_{\max} J_o\left(k\sqrt{x^2 + y^2}\right) \times \left[1 - \exp\left(-t^2 / \tau^2\right)\right] \quad (4)$$

where r is radius, r<(2.4048)/k, and τ = 0.5 L_z/W_o.

3.3. Control Run and Suite of Experiments

The control run (CR) closely approximates DJ08's simulation, except with a full circular plane of hydrometeors and q_{max} = 5 g kg^{-1} (Fig. 4a). It is run for 3000 s. The results of CR are used to verify that the model set-up herein closely resembles that of DJ08 as much as possible. They are also used for comparison and analysis with the other experiments.

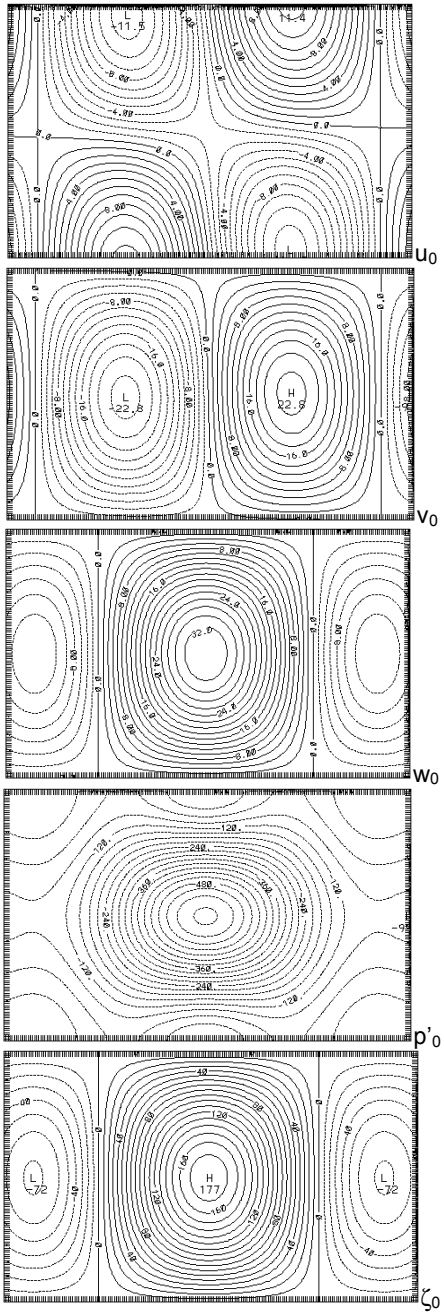

Fig. 3: Initial Beltrami flow. Units of u_0, v_0, and w_0 are m s^{-1}. Units of p'_0 are Pa. Units of ζ'_0 are s^{-1}. The inteval Δu_0 = 1 m s^{-1}; Contour intervals of v_0 = 2 m s^{-1}; contour intervals w_0 = 2 m s^{-1}; contour intervals p'_0 = 30 Pa; and contour intervals ζ'_0 = 1.0 x 10^{-3} s^{-1}.

The first suite of experiments is designed to investigate the influence of the amount of precipitation in the descending rain curtain on tornadogenesis and tornado strength. In these experiments, the axisymmetric rain curtain is retained, and q_{max} is set to 1 g kg^{-1}, 3 g kg^{-1}, 7 g kg^{-1}, and 9 g kg^{-1} in four separate simulations (Fig 4a). (Hereafter, these will be referred to as C1, C3, C7, and C9, respectively.) These simulations each are run for 3000 s. A run without rain (q_{max} = 0 g kg-1) was also done. The results of this simulation are not included because the flow remained in steady state. DJ08 also demonstrated that the barotropic mechanism of tornadogenesis fails without precipitation in his axisymmetric model as it also does in the three-dimensional model.

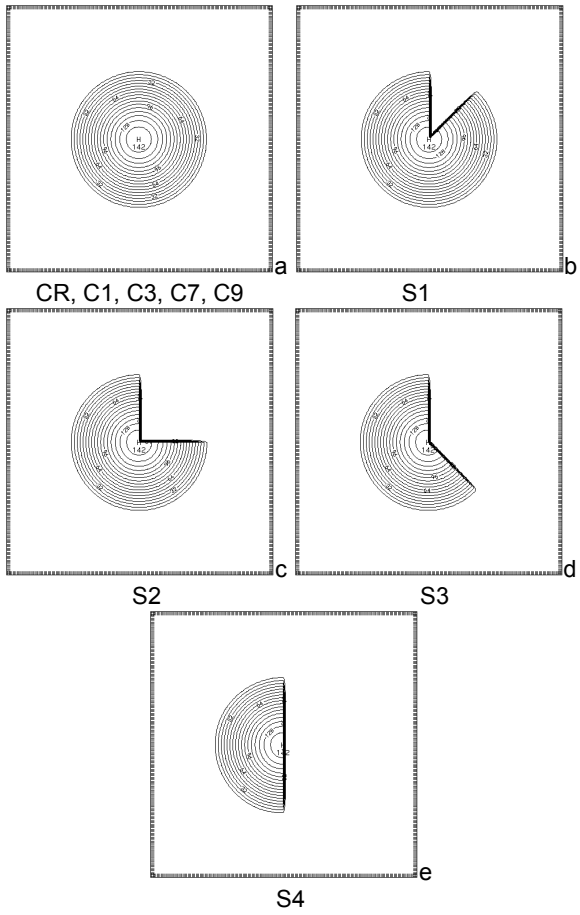

Fig. 4: Initial rain curtains in experiments CR, C1, C3, C7, C9 (a); S1 (b); S2 (c); S3 (d); and S4 (e). at t=0. Contours are of q. Units of q are g kg^{-1}.

The second suite of experiments tests a proxy for how far the hook echo must wrap around the updraft for tornadogenesis to occur. In these experiments, q_{max} is restored to 5 g kg^{-1}. The horizontal, circular plane of hydrometeors is successively reduced, by 45-degree increments (i.e. eighths), from the full circular plane used in CR to a half-circle. In the first experiment (hereafter S1) the rain curtain wraps 315 degrees around the updraft (i.e. seven-eighths) (Fig 4b). This is reduced to 270 degrees (i.e. three-quarters), 225 degrees (i.e. five-eighths), and 180 degrees (i.e. one-half) in experiments labeled S2 (Fig. 4c), S3 (Fig. 4d), and S4 (Fig. 4e), respectively. These simulations are each run for 3600 s.

4. RESULTS

DJ08 defined a mesocyclone as a cyclonic vortex with core radius greater than two kilometers, a tornado cyclone (TC) as a cyclonic vortex with core radius less than two kilometers that does not break the thermodynamic speed limit, and a tornado as a cyclonic vortex with core radius less than two kilometers that does break the thermodynamic speed limit. These same definitions will be used in this study. This study also defines an incipient tornado as a cyclonic vortex with core radius less than two kilometers, which forms within the TC and evolves directly into the tornado.

4.1. Control Run

After their release, the hydrometeors diverge away at the top of the updraft, and descend as a precipitation-driven annular rain curtain through the updraft-downdraft interface. As the rain curtain descends, it is advected cyclonically around the rotating updraft, creating a "twisting" downdraft (Fujita 1973) as in DJ08 (Fig 5a). The rain curtain passes through air with high angular momentum, and drags this air towards the surface. Inflow causes the rain curtain to curve slightly inwards beneath the mid-level mesocyclone as it descends. The rain curtain reaches the ground at about 1080 s (shown at 300 m above the surface in Fig 6a) and converges inward due to both mass conservation and radial inflow (Fig 5b and Fig. 6b). Cyclonic flow is maintained as hydrometeors converge towards the low-level updraft (Fig. 6c, d).

As the rain curtain reaches the ground, the air enters the updraft (Fig. 5c, d). Angular momentum is drawn inwards, increasing tangential acceleration beneath the mid-level mesocyclone and producing positive vertical vorticity. The air is recycled upwards by the updraft, which amplifies the positive vertical vorticity through stretching. Consequently, the mid-level mesocyclone spins-up slightly (~ 3.5 x 10-2 s^{-1}).

Establishment of cyclostrophic balance is attempted as tangential acceleration increases within the updraft below mid levels. Pressure accordingly decreases, driving a stronger radial component of the flow. This draws more high angular momentum air into the updraft, enhancing the process and increasing rotation below mid levels. As convergence of angular momentum beneath the mid-level mesocyclone continues, a TC develops at about 1860 s as a downward extension of the mid-level mesocyclone (Fig. 7a).

At about 2160 s, an incipient tornado develops independently of the mid-level mesocyclone and TC. The incipient tornado develops at about 1.5 km above the surface as convergence and recycling of the high angular momentum air are maximized at and just above the surface (Fig. 7b). It lowers towards the surface and contracts into a tornado at about 2310 s (Fig 7c). Its maximum strength is reached between 2460 s and 2490 s (Fig. 7d), and is characterized by intense upward motion of 131.7 m s^{-1} (nearly four times stronger than the thermodynamic speed limit), ζ' of 1.37 s^{-1}, radial inflow over 100 m s^{-1}, and a pressure deficit of 11216.5 Pa (nearly 20 times larger than the initial deficit in the mid-level mesocyclone).

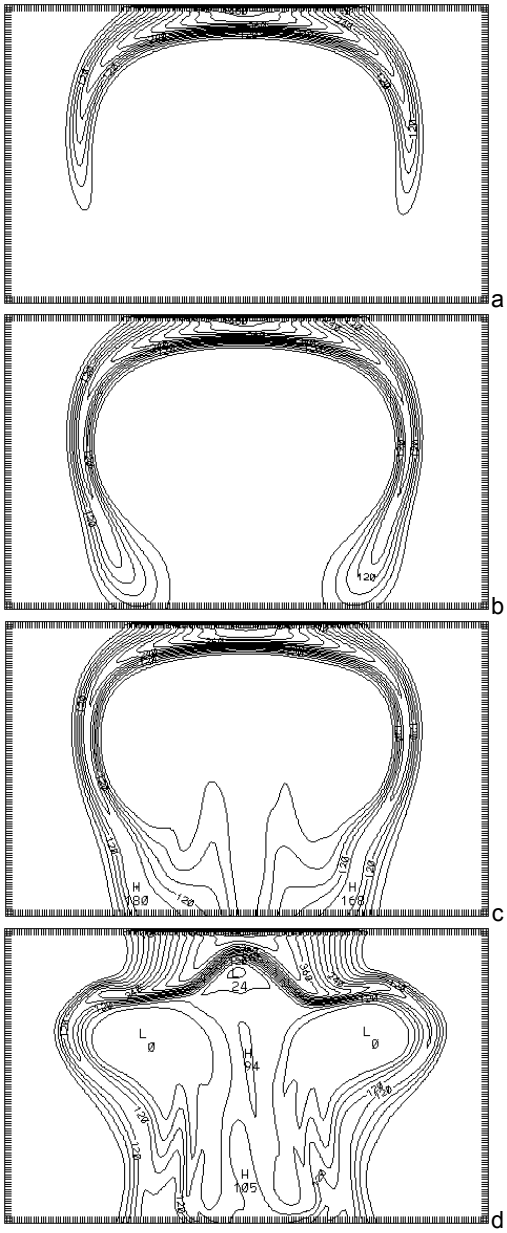

Fig. 5: Evolution of the descending rain curtain, as viewed from a vertical slice through the center of the domain at 720 s (a); 1100 s (b); 1470 s (c); and 2130 s (d). Contours are of q. Contour intervals of q = 4.0 x 10^{-4} g kg^{-1}.

Starting at 2490 s, an axial downdraft proceeds from the top of the storm through the updraft owing to the downward directed vertical pressure gradient and causes the tornado to evolve into a two-celled structure before dissipating the tornado. Shortly afterwards, rain falling in to the weakened updraft

collapses the entire storm. This sequence of events is close to those that proceed in DJ08's experiment.

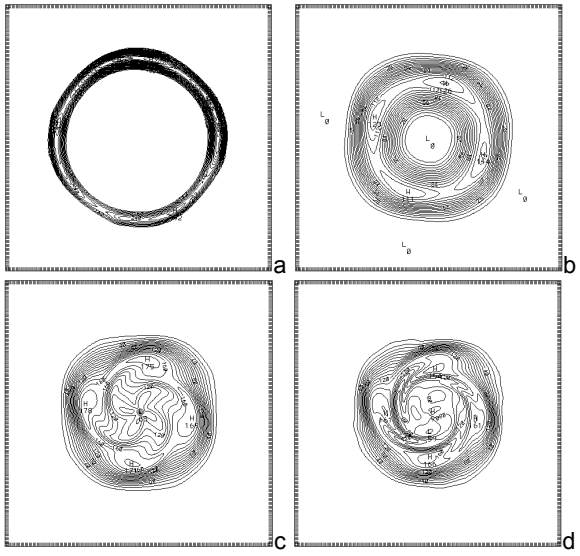

Fig. 6: Evolution of the descending rain curtain in CR, as viewed from a horizontal slice at z = 300 m above the ground, at: 600 s (a); 1200 s (b); 1890 s (c) and 2220 s (d). Contours are of q. Contour intervals of q = 1.0 x 10^{-5} g kg^{-1}.

4.2. Circular Rain Curtain Experiments

Tornadogenesis fails in C1 and C3 as descending rain curtains with small mixing ratios are unable to transport to the surface and converge sufficient amounts of angular momentum for tornadogenesis. Thus, these experiments will not be discussed in the results.

The C7 and C9 simulations both produce tornado-strength vortices. Qualitatively, these experiments behave as CR. However, the precipitation-driven downdrafts are stronger relative to CR, and substantially more angular momentum is converged near the surface. This results in more rapid tornadogenesis relative to CR (Fig. 8).

In C7, the TC forms at about 1620 s. The incipient tornado develops at about one kilometer above the ground simultaneously, although independent of the mid-level mesocyclone and TC. The incipient tornado descends and contracts into a tornado at about 1710 s. In C9, the TC forms at about 1530 s. Again, development of an incipient tornado at about 800 meters above the ground is nearly simultaneous and independently, and the mid-level mesocyclone and TC. Tornadogenesis succeeds at about 1860 s.

More rapid tornadogenesis does not, however, translate into stronger tornadoes in the simulations. Maximum values of ζ', -p', and w are compared in Table 3. Tornado-strength vortices in C7 and C9 are much weaker than CR. This is because more energy is expended to overcome greater precipitation drag and loft the precipitation-laden air. The vortices are also broader than in CR.

The axial downdrafts in C7 and C9 are stronger than the axial downdraft in CR (Fig 9). Their maximum downward velocities of 53 m s^{-1} (C7) and 51.1 m s^{-1} (C9) are roughly 15 m s^{-1} faster than in CR. Since the downward directed vertical pressure gradient is stronger in CR than in C7 and C9 (not shown), the stronger velocities must be attributed to greater precipitation drag (water loading).

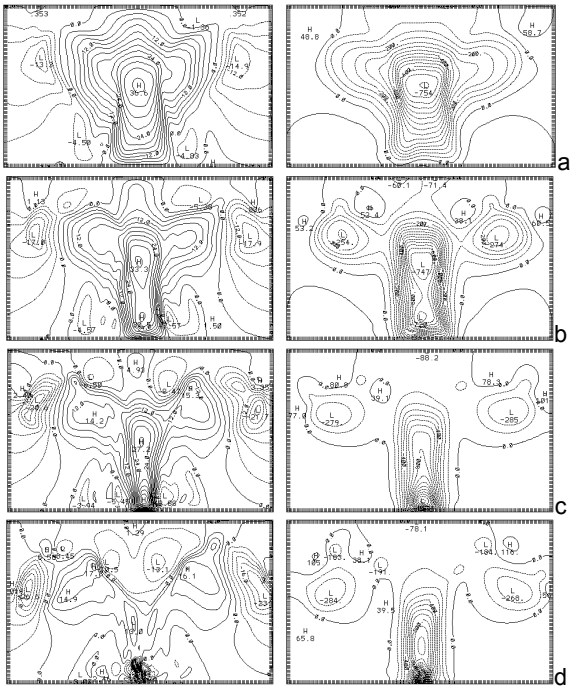

Fig. 7: Vertical motion w (left panels) and pressure perturbation p' (right panels) for CR at: 1860 s (a); 2160 s (b); 2310 s (c); and 2460 s (d). Units of w are m s^{-1}. Units of p' are Pa. Contour intervals of w = 4 m s^{-1}. Contour intervals of p' = 50 Pa in a and b, and 100 Pa in c and d.

	Max{ζ'} (s^{-1})	Max{-p'} (Pa)	Max{w} (m s^{-1})
CR	1.372	11216.49	131.74 (3.9)
C7	0.789	4068.92	58.91 (1.7)
C9	0.514	1057.62	46.48 (1.4)
S1	0.728	2973.96	59.62 (1.8)
S2	0.538	1658.51	50.73 (1.5)
S3	0.357	879.87	41.84 (1.2)

Table 3: Maximum values in the tornado-like vortices of ζ', -p', and w. In parentheses in the Max{w} column is the multiple by which the maximum wind speed exceeds the thermodynamic speed limit W_o.

4.3. Asymmetric Rain Curtain Experiments

The asymmetric configuration of the initial plane of hydrometeors in S1, S2, S3, and S4 greatly disrupts the structure of the parent supercell. As the

rain curtain descends along the updraft-downdraft interface, a horizontal gradient in precipitation drag causes the storms to develop tilt with height. Tilt increases as more slices are removed from the circular plane of hydrometeors in S1, S2, S3, and S4, respectively.

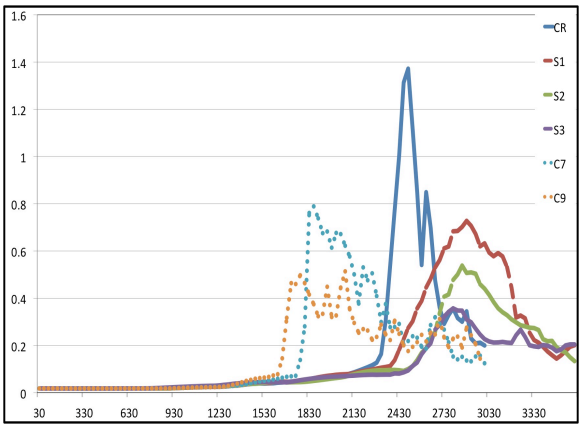

Fig. 8: Positive perturbation vertical vorticity plotted against time. The x-axis (time) goes from 30 s to 3000 s, with Δt = 30 s. The y-axis (ζ') goes from 0 s^{-1} to 1.6 s^{-1}, with $\Delta\zeta$ = .2 s^{-1}. CR is in solid blue, C7 is in dotted turquoise, and C9 is in dotted orange.

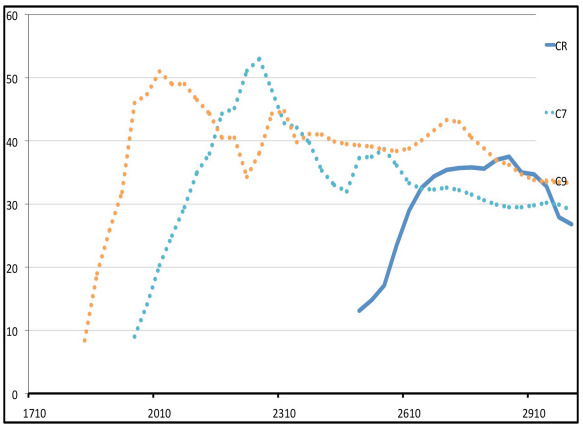

Fig. 9: Downward vertical motion plotted against time. The x-axis (time) goes from 1710 s to 3000 s, with Δt = 30 s. The y-axis (-w) goes from 0 m s^{-1} to 60 m s^{-1}, with Δ(-w) = 10 m s^{-1}. CR is in solid blue, C7 is in dotted turquoise, and C9 is in dotted orange.

In these experiments, the descending rain curtain is advected cyclonically due to the influence of the rotating updraft (example from S2 in Fig. 10a, b), and eventually encircles the updraft. As it reaches the surface, the cyclonic flow converges (Fig 10c, d), and the precipitation-laden air enters the updraft and is recycled upwards. As the simulations progress, the experiments look qualitatively similar near the surface to CR, with rain wrapping cyclonically around and eventually surrounding the developing tornadic circulation (Fig 10c, d).

More time is needed relative to CR for sufficient precipitation to converge and for angular momentum to converge and recycle upwards into the developing tornado, and tornadogenesis is delayed (Fig. 11). Tornadogenesis occurs in S1 at 2400 s; 2490 s in S2; and 2610 s in S3. In S4, insufficient precipitation is available for this mechanism, and tornadogenesis fails. Thus, this experiment will not be further included in the results.

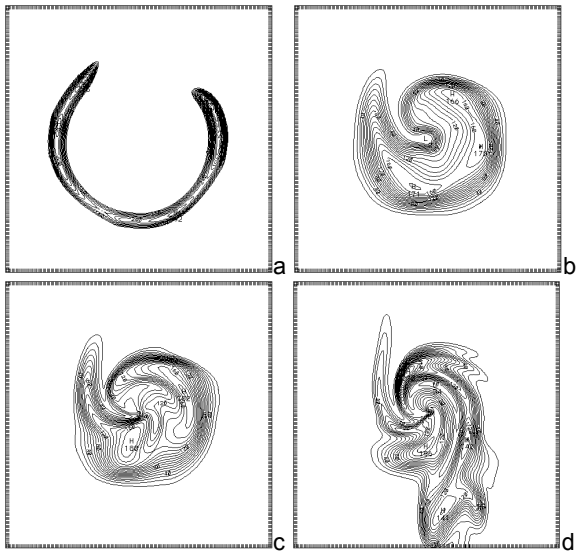

Fig. 10: Evolution of the descending rain curtain in S2, as viewed from a horizontal slice at z = 300 m above the ground, at: 600 s (a); 1530 s (b); 2100 s (c) and 2520 s (d). Contour of q = 1.0 x 10^{-5} g kg^{-1}.

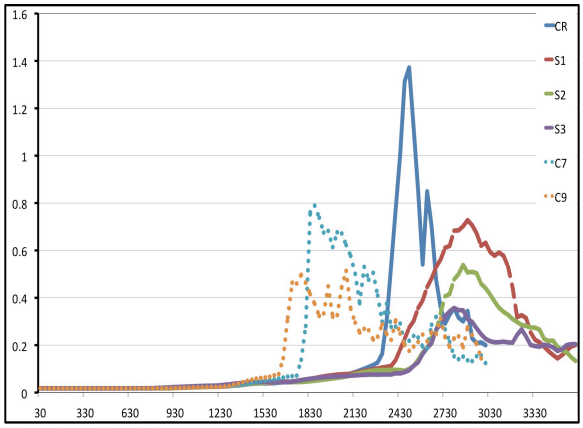

Fig. 11: Positive perturbation vertical vorticity plotted against time. The x-axis (time) goes from 30 s to 3000 s, with Δt = 30 s. The y-axis (ζ') goes from 0 s^{-1} to 1.6 s^{-1}, with $\Delta\zeta$ = .2 s^{-1}. CR is in solid blue, C7 is in dotted turquoise, C9 is in dotted orange, S1 is in dashed red, S2 is in dashed green, and S3 is in dashed purple.

It is in this suite of experiments that the development of asymmetries in a three-dimensional model is most apparent. Because of the initial asymmetry of the rain curtain, convergence of

precipitation is preferred on a certain side of the storm, and the storm tilts with height towards the side of the storm with more precipitation. The TC also tilts with height as it develops. The incipient tornado develops about one-half kilometer above ground level higher than in CR, but still forms independently of the mid-level mesocyclone, and on the side of the storm with more descending precipitation. Tornadogenesis is also skewed away, to the stronger gradient of upward/downward vertical motion, which is towards the side of the storm with more precipitation.

The three tornado-producing experiments are similar, but tornado strength weakens as more slices are removed from the circular rain curtain (Table 3). Radial inflow is significantly weaker, inhibiting penetration and concentration of angular momentum into the tornadic region. In each case, the maximum vertical velocity in the tornadoes is less than half of the CR. The maximum pressure deficits in the tornadoes are 26.5% (S1), 14.8% (S2), and 7.76% (S3) of the maximum pressure deficit in CR.

Because of the skewed configuration of the storm and tornado, axial downdrafts do not form in S1, S2, or S3. The tornadoes maintain their single cell structure, and travel away from their points of origin to roughly the northwest (top-left) quadrant of the domain.

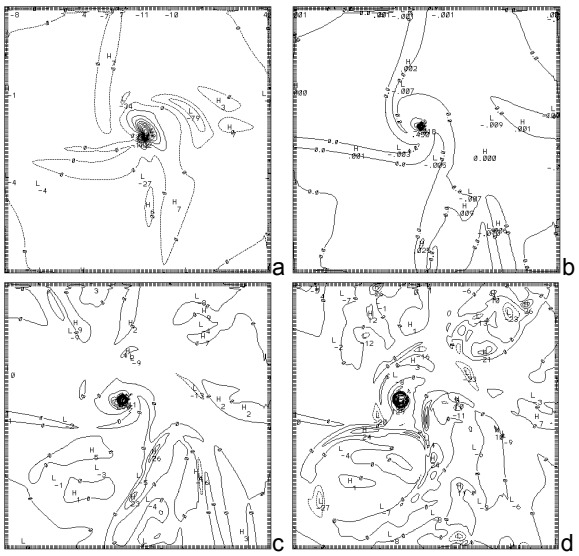

Fig. 12: Travel of tornado away from point of origin in S2, as viewed from a horizontal slice at z = 300 m above the ground, at: 2280 s (a); 2880 s (b); 3180 s (c) and 3480 s (d). Contours are of $\zeta' = 1.0 \times 10^{-3}$ s^{-1}.

5.SUMMARY AND CONCLUSIONS

DJ08 used an axisymmetric model to simulate tornadogenesis by descending rain curtains. The mechanism is purely barotropic, and in general describes Fujita's Recycling Hypothesis.

The study described herein extends DJ08 into three dimensions, with the added dimension permitting asymmetric features like storm tilt to develop. The control run closely reproduces DJ08's simulation and confirms his results.

In two suites of experiments, properties of the descending rain curtain were varied, and their effects on tornadogenesis were examined. The first suite maintained the initially circular rain curtain and varied the mixing ratio among low, moderate, and high values. The second suite created initially asymmetric rain curtains by removing 45-degree slices from a circular rain curtain. For these simulations, a moderate mixing ratio was retained.

Descending rain curtains with small mixing ratios transport downwards insufficient angular momentum for tornadogenesis. Descending rain curtains with large mixing ratios increase downward angular momentum transport by creating stronger precipitation-driven downdrafts. While increased precipitation causes earlier tornadogenesis relative to less precipitation, these scenarios produce broader, weaker tornado-like vortices than with a moderate mixing ratio. Increased precipitation drag with large mixing ratios also drives stronger axial downdrafts.

An initially asymmetric rain curtain affects storm features that in turn influence tornadogenesis and the ensuing tornadoes. A gradient of precipitation drag across the storm promotes storm tilt with height. Because the updraft is skewed from the region of maximum convergence at the surface, upward recycling of hydrometeors and angular momentum is hindered. This delays tornadogenesis relative to simulations with initially circular rain curtains, and offsets the resulting tornadoes from the center of the updraft to the updraft side of the gradient between upward and downward vertical motion. Because the tornado is skewed from the center of the updraft, it is possible that an axial downdraft might not form. Thus, the tornado is not dissipated, and instead travels away from its point of origin.

The results of this study suggest that Fujta's Recycling Hypothesis demonstrates strong potential for explaining tornadogenesis in environments where the DPE fails. The suites of experiments performed herein begin to examine this mechanism of tornadogenesis in less-than-ideal—and therefore, increasingly realistic—environments.

Acknowledgements: The authors would like to thank Robert Davies-Jones and Alan Shapiro for helpful discussions. We are delighted and grateful to Craig Schwartz for his help with scripting. This work was supported by the National Science Foundation (NSF) grants ATM 0446509 and 0733539.

REFERENCES

Davies-Jones R. 1982a. Observational and theoretical aspects of tornadogenesis. In Topic in Atmospheric and Oceanographic Sciences: Intense Atmospheric Vortices, Bengtsson L, Lighthill J (eds). Springer Verlag: New York; 175 – 189.

Davies-Jones R. 1982b. A new look at the vorticity

equation with application to tornadogenesis [preprints, 12th Conference on Severe Local Storms]. American Meteorological Society, Boston, MA; 249 – 252.

Davies-Jones R. P., and H. E. Brooks, 1993: Mesocyclogenesis from a theoretical perspective. The Tornado: Its Structure, Dynamics, Prediction, and Hazards, Geophys. Monogr., Vol. 79, Amer. Geophys. Union, 105–114.

Davies-Jones, R., 2008: Can a Descending Rain Curtain in a Supercell Instigate Tornadogenesis Barotropically? *J. Atmos. Sci*., **65**, 2469–2497.

Fiedler, B. H., and R. Rotunno, 1986: A theory for the maximum windspeed in tornado-like vortices. *J. Atmos. Sc*i., **43**, 2328–2340.

Fujita, T. T., 1973: Proposed mechanism of tornado formation from rotating thunderstorm. Preprints, Eighth Conf. on Severe Local Storms, Denver, CO, Amer. Meteor. Soc., 191-196.

Fujita T. T., 1975: New evidence from the April 3–4, 1974 tornadoes. Preprints, Ninth Conf. on Severe Local Storms, Norman, OK, Amer. Meteor. Soc., 248–255.

Klemp, J. B., Rotunno, R., 1983: A study of the tornadic region within a supercell thunderstorm. *J. Atmos. Sc*i., **40**, 359-377.

Klemp, J. B., and R. Wilhelmson, 1978: The simulation of three-dimensional convective storm dynamics. *J. Atmos. Sci*., **35**, 1070-1096.

Leslie, L. M., 1971: The development of concentrated vortices: A numerical study. *J. Fluid Mech*., **48**, 1–21.

Lewellen, D. C., and W. S. Lewellen, 2002: Near-surface intensification during unsteady tornado evolution. Extended Abstracts, 21st Conf. on Severe Local Storms, San Antonio, TX, Amer. Meteor. Soc., 12.8, 1-4.

Lewellen, D.C., and W.S. Lewellen, 2007: Near-Surface Intensification of Tornado Vortices. *J. Atmos. Sci.*, **64**, 2176–2194.

Lewellen, W. S., D. C. Lewellen, and Sykes, R.I., 1997: Large-eddy simulation of a tornado's interaction with the surface. *J. Atmos. Sci*., **54**, 581-605.

Markowski P. A., J. M. Straka, and E. N. Rasmussen, 2002: Direct surface thermodynamic observations within the rear-flank downdrafts of nontornadic and tornadic supercells. *Mon. Wea. Rev*., **130**, 1692–1721.

Markowski P. M., 2002: Hook echoes and rear-flank downdrafts: A review. *Mon. Wea. Rev*., **130**, 852–876.

Markowski, P. M, Straka, J. M., and Rasmussen, E. N. (2003): Tornadogenesis Resulting from Transport of Circulation by a Downdraft: Idealized Numerical Simulations. *J. Atmos. Sci*., **60**, 795–823.

Rasmussen E. N., J. M. Straka, R. Davies-Jones, C. A. Doswell, F. H. Carr, M. D. Eilts, and D. R. MacGorman, 1994: Verification of the Origins of Rotation in Tornadoes Experiment: VORTEX. *Bull. Amer. Meteor. Soc*., **75**, 995–1006.

Rotunno R., and J. B. Klemp, 1985: On the rotation and propagation of simulated supercell thunderstorms. *J. Atmos. Sci*., **42**, 271–292.

Shabbott, C.J., and P.M. Markowski, 2006: Surface In Situ Observations within the Outflow of Forward-Flank Downdrafts of Supercell Thunderstorms. *Mon. Wea. Rev*., **134**, 1422–1441.

Smith, R. K., and L. M. Leslie, 1978: A numerical study of tornadogenesis in a rotating thunderstorm. *Quart. J. Roy. Meteor. Soc*., **105**, 107–127.

Trapp, R. J., E. D. Mitchell, G. A. Tipton, D. A. Effertz, A. I. Watson, D. L. Andra, and M. A. Magsig, 1999: Descending and non-descending tornadic vortex signatures detected by WSR-88D's. *Wea. Forecasting*, **14**, 625-639.

Trapp, R. J., and R. Davies-Jones, 1997: Tornadogenesis with and without a dynamic pipe effect. *J. Atmos. Sci.*, **54**, 113-133.

Trapp, R.J., G.J. Stumpf and K.L. Manross, 2005: A Reassessment of the Percentage of Tornadic Mesocyclones. *Wea. Forecasting,* **20**, 680-687.

Walko, R. L., 1993: Tornado spin-up beneath a convective cell: Required basic structure of the near-field boundary layer winds. The Tornado: Its Structure, Dynamics, Prediction and Hazards, Geophys. Monogr., No. 79, Amer. Geophys. Union, 89–95.